Using the Graphene Moiré Pattern for the Trapping of C_{60} and Homoepitaxy of Graphene

Jiong Lu,[†,‡] Pei Shan Emmeline Yeo,[†,§] Yi Zheng,[†,‡] Zhiyong Yang,[†] Qiaoliang Bao,[†] Chee Kwan Gan,[§] and Kian Ping Loh[†,‡,*]

[†]Department of Chemistry, National University of Singapore, 3 Science Drive 3, Singapore 117543, [‡]Graphene Research Centre, National University of Singapore, 2 Science Drive 3, Singapore 117542, and [§]Institute of High Performance Computing, 1 Fusionopolis Way, #16-16 Connexis, Singapore

ABSTRACT

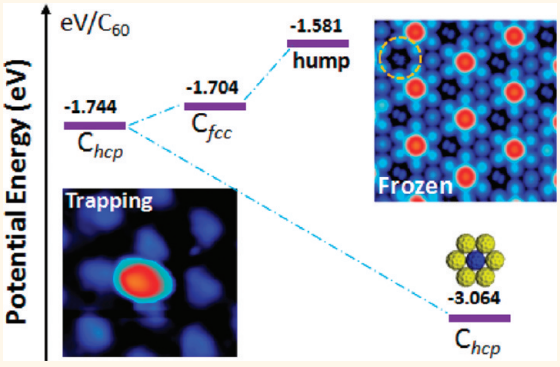

The graphene Moiré superstructure offers a complex landscape of humps and valleys to molecules adsorbing and diffusing on it. Using C_{60} molecules as the classic hard sphere analogue, we examine its assembly and layered growth on this corrugated landscape. At the monolayer level, the cohesive interactions of C_{60} molecules adsorbing on the Moiré lattice freeze the molecular rotation of C_{60} trapped in the valley sites, resulting in molecular alignment of all similarly trapped C_{60} molecules at room temperature. The hierarchy of adsorption potential well on the Moiré lattice causes diffusion-limited dendritic growth of C_{60} films, as opposed to isotropic growth observed on a smooth surface like graphite. Due to the strong binding energy of the C_{60} film, part of the dentritic C_{60} films polymerize at 850 K and act as solid carbon sources for graphene homoepitaxy. Our findings point to the possibility of using periodically corrugated graphene in molecular spintronics due to its ability to trap and align organic molecules at room temperature.

KEYWORDS: molecular assemblies · graphene Moiré template · potential well · C_{60} molecular array · homoepitaxy of graphene

Tailoring the arrangement of organic nanostructures on graphene is important to realize its potential as a template for molecular electronics.[1−5] The assembly mechanism of organic molecules on graphene is distinct from bulk graphite due to the low density of step edges on chemically vapor deposited graphene, as well as the presence of periodic corrugations on graphene grown epitaxially on metal.[6] A rich spectrum of growth mechanisms is possible in organic film growth because of the anisotropy of organic molecules.[3,4,7,8] Molecular packing of organic molecules on an inert substrate is affected by their internal degrees of freedom.[9] In addition, steric and electronic interactions also decide the spatial conformations of the molecules and how they undergo 2D crystallization. Different polymorphism of the same molecular film can exist depending on molecule−substrate or molecule−molecule interactions. One general approach to form a well-ordered molecular assembly is based on intermolecular interactions such as hydrogen bonds, ionic bonds, and $\pi-\pi$ stacking to allow high-symmetry ordering with selectivity and directionality.[1,7,8] However, the molecular assembly of highly symmetrical molecules such as C_{60} molecules requires another strategy, since the molecules lack ligands for highly directional bonding. In addition, C_{60} has low-energy barriers of surface migration on inert substrates, and its rotational energy barrier is on the order of a few tenths of a meV; thus it is highly mobile on a flat and inert substrate such as graphite at room temperature (RT).[10,11] In this case, the growth of C_{60} films is governed mainly by thermodynamics, which favors the isotropic growth of round and compact nanostructures close to thermodynamic equilibrium.[12] It is well known that the in-plane compressive stress arising from the lattice mismatch of a graphene monolayer grown on metal gives rise to a highly corrugated surface known as the Moiré superlattice.[13] It is interesting to consider how a corrugated landscape affects the assembly and packing of a highly symmetrical, spherical molecule such as C_{60}, which can be viewed as a model for a hard-sphere

* Address correspondence to chmlohkp@nus.edu.sg.

Received for review November 22, 2011 and accepted December 23, 2011.

Published online December 23, 2011
10.1021/nn204536e

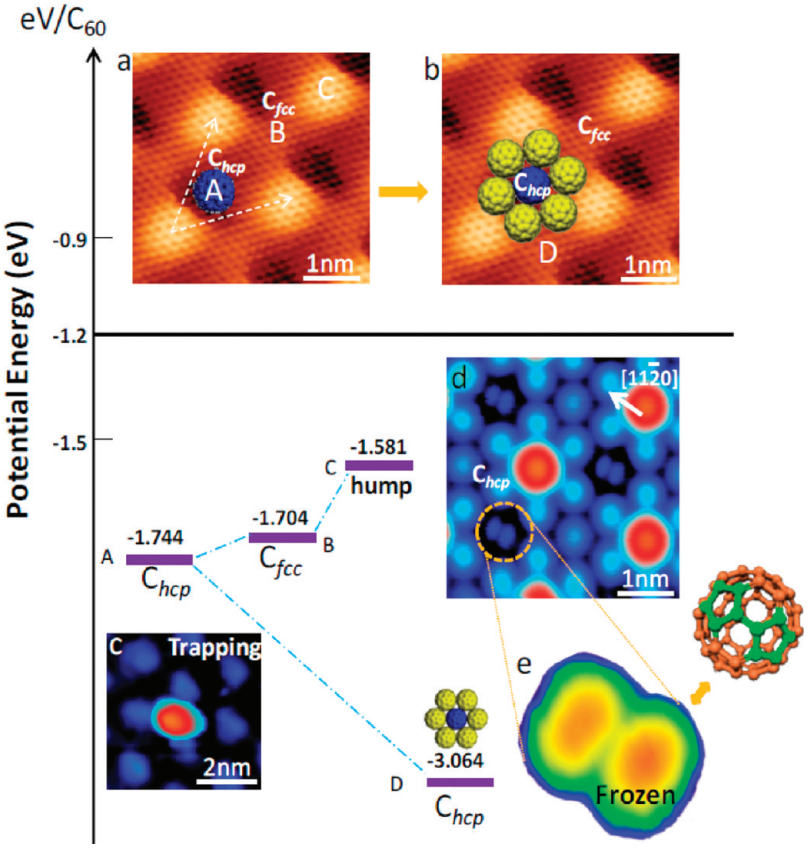

Figure 1. Hierarchical adsorption energies of C_{60} molecules in different sites of the graphene Moiré pattern. (a) Scheme of an individual C_{60} molecule preferentially trapped in the C_{hcp} valley at RT and its corresponding STM image as shown in (c). (b) Scheme of six C_{60} molecules attached to the trapped C_{60} as a seed for the nucleation of monolayer C_{60} islands; C_{60}–C_{60} cohesive energy increases. (d) RT freezing of the thermal motions of C_{60} in the C_{hcp} valleys once a C_{60} monolayer is formed. (e) All C_{60} molecules trapped in C_{hcp} valleys display a dumbbell shape, aligning along the $\langle 11\bar{2}0 \rangle$ directions. The bright lobes in the dumbbell-shaped correspond to pentagons of the C_{60} cage at positive sample bias, which suggests C_{60} orients with the 6:6 bond (the C–C bond between two carbon hexagons) facing upward, as shown in the right top of (e).

close-packing arrangement. We discover that the Moiré surface presents a unique diffusion barrier that restricts the surface mobility of C_{60} due to the presence of humps and valleys. In this case, nonequilibrium shape evolution occurs and kinetic control provides an elegant way to manipulate the growth morphologies of C_{60}, as well as nanostructures derived from the decomposition of its assembled film.

RESULTS AND DISCUSSION

Graphene exhibits an ordered Moiré pattern with a lattice constant of ~30 Å on Ru(0001). Due to the buckling instability on Ru, some carbon atoms are displaced vertically from the substrate, forming a graphene landscape of humps and valleys, as shown in the STM image of graphene on Ru(0001) (Figure 1a,b). The hump regions correspond to the brightest regions in the STM image and consist of almost free-standing graphene nanoislands, while the valley regions consist of graphene chemically hybridized to the Ru substrate.[14] The valley regions in one unit cell can be divided into two parts (A and B, as indicated in Figure 1a) depending on how graphene is oriented with respect to the Ru substrate below. In valley A (darkest region in the STM image), three atoms in a hexagonal ring of graphene occupy the hexagonal-close-packed (hcp) interstitial sites, with the other three atoms sitting directly on top of a Ru atom. This valley is known as the C_{hcp} valley.[15,16] In valley B (Figure 1a), three atoms in the hexagonal ring of graphene occupy the face-centered-cubic (fcc) interstitial sites of Ru(0001), while the other three atoms sit directly on top of a Ru atom. This region shall henceforth be termed the C_{fcc} valley. The chemical hybridization between carbon atoms in the valley regions and Ru(0001) results in a back-donated charge transfer to graphene and results in the electron doping of the valley region.[17,18] The electron enrichment of the valley region increases its reactivity to adsorbates, as will be shown later.

Such a corrugated superlattice has pronounced influences on the assembly of C_{60} molecules. To investigate its effects, a sequence of STM images were recorded during the growth of C_{60} nanoislands from the submonolayer to multilayer regime, as shown in Figure 3. Judging from the sequential order in the occupation of

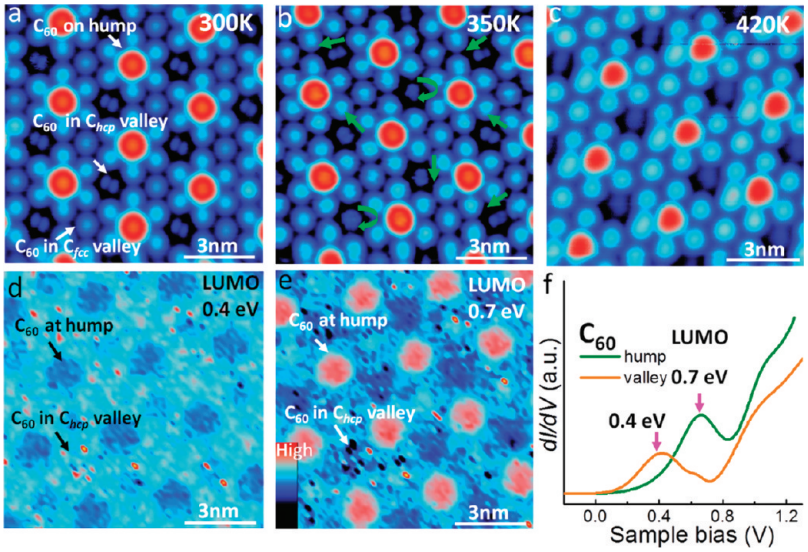

Figure 2. Molecularly oriented dumbbell-shaped features in the STM image for C_{60} molecules sitting in the C_{hcp} valley (a) at 300 K. (b) In-plane rotation (spinning) of C_{60} molecules occurs at 350 K, resulting in disordered fuzzy dumbbell-shaped C_{60} molecules; coverage = 0.8 ML. (c) Out-of-plane rotation is thermally activated at 420 K and the dumbbell shape vanishes. d*I*/d*V* mapping of unoccupied states of C_{60} molecules (d) at 0.4 eV and (e) at 0.7 eV. (f) STS spectra of C_{60} molecules on humps (dark green) and in valleys (orange). Tunneling parameters: (a−c) V = 1.2 V, I = 0.1 nA.

adsorption sites, we can see that there is a hierarchy in the adsorption energies associated with these sites in the Moiré template. At a low coverage of 0.04 ML, an individual C_{60} molecule (red spot in Figure 1c) is observed to be trapped exclusively in the C_{hcp} valleys instead of C_{fcc} valleys. At this stage, the trapped C_{60} molecule can rotate freely, as judged from the rounded hemispherical protrusion in the STM image. Once the C_{hcp} valley is populated by seven C_{60} molecules to form a heptamer (Figure 1b), the population of neighboring sites occurs, and these follow a hierarchical order, beginning with the occupation of the C_{fcc} sites, followed by adsorption on the highest points of the humps, and finally the adsorption of six C_{60} molecules around the circumference of the humps (Figure 1d and Figure 2a). When the coverage of C_{60} molecules is increased from 0.04 to 0.4 ML, highly uniform dumbbell shapes are now imaged for all the C_{60} molecules occupying the C_{hcp} valleys (Figure 1d). The dumbbell shape is due to the C_{60} molecules adopting a structure with its 6:6 bond (the C−C bond between two carbon hexagons) facing up, as shown in Figure 1e.[19,20] This indicates that molecular rotations are frozen at RT once a "crowding effect" by neighboring C_{60} occurs. The in-plane orientational ordering of C_{60} molecules in the C_{hcp} valleys is stable up to 350 K, beyond which the two-dimensional rotation (spinning) is thermally excited and in-plane disorder results. Out-of-plane molecular rotation occurs at 420 K, as can be seen from the smearing out of the dumbbell shape into a hemisphere for the C_{60} molecules in the C_{hcp} valleys.

Density-functional theory (DFT) simulations were performed to investigate the adsorption energies of C_{60} molecules on microscopically distinct regions such as C_{hcp} and C_{fcc} valleys and graphene humps. The results show that the adsorption energies of these different sites are sufficiently distinct, from the highest energy (most exothermic) for C_{60} in the C_{hcp} valleys (−1.744 eV) to the lowest energy for C_{60} at the humps (−1.581 eV), as displayed in Figure 1. Thermal desorption studies reveal that C_{60} molecules desorb from the multilayer at 480 K, and complete desorption of the monolayer occurs at 550 K using a linear heating ramp (0.2 K/s). From this, the desorption energy of C_{60} is estimated to be ∼1.5 eV on the basis of the desorption rate for an isolated species[7,21] $\Gamma_{des} = \nu_o \exp[-E/k_BT]$, where ν_o is on the order of 10^{-13} s^{-1}.

Therefore, the average binding of C_{60} molecules on the graphene Moiré template is stronger than graphite, as the maximum binding energy reported for C_{60} molecules on the latter is ∼1 eV.[11,12] The potential energy variation (from highest to lowest potential energy) on a flat graphite surface is −13 meV since all sites are more or less equivalent; this explains why C_{60} molecules are highly mobile on graphite at RT.[10,11] In contrast, the potential barrier for migration between two different sites on a graphene Moiré pattern will be more than or equal to the difference in adsorption energies between these two different sites. The energy variation between the hump and C_{hcp} valley is 163 meV, which exceeds the thermal energies ($k_BT \approx 25.7$ meV) at RT. Therefore, the surface migration of C_{60} is inhibited at RT and C_{60} will be trapped in surface potential wells. However, the trapped C_{60} still has a spinning motion (rotation about the axis perpendicular to the surface) since the energy barrier of spinning is very small, on the order of a few meV, which increases with the binding energy of C_{60} molecules. Additional binding

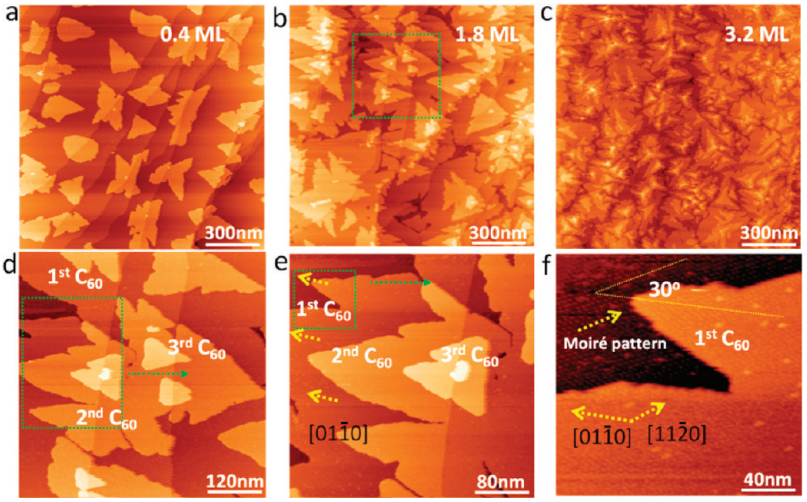

Figure 3. Dentritic growth of C_{60} islands on graphene/Ru(0001). Increased coverage of C_{60} from (a) 0.4 ML, to (b) 1.8 ML, to (c) 3.2 ML. (d) Magnified view is marked by a green dashed square in (b). (e) Magnified view shows that the dentritic growth of the second layer C_{60} islands is aligned with the first layer C_{60} islands and that the third layer is compact. (f) Magnified view of green-dotted region in (e) reveals that the growth front of the first layer dentritic C_{60} islands rotates by 30° with respect to the $\langle 11\bar{2}0\rangle$ directions in the graphene Moiré superlattice. Tunneling parameters (a–f): V = 1.2 V, I = 0.1 nA.

energy of C_{60} is contributed by the cohesive energy arising from intermolecular van der Waals interactions (0.22 eV per C_{60}–C_{60}). The maximum coordination number of each C_{60} in the monolayer film is 6. Therefore, C_{60} adsorbed on the C_{hcp} site gains ~1.32 eV in binding energy at full coverage, which significantly increases the energy barrier for molecular spinning in the C_{hcp} site over thermal energy at RT,[22] as shown in Figure 1d and Figure 2a.

Insight into the trapping of the C_{60} in the C_{hcp} valleys can also be derived from the differences in the electronic characteristics of C_{60} adsorbed on the humps and valleys, which we have investigated using STS. The features in Figure 2f located at 0.4 and 0.7 eV correspond to the LUMO states for C_{60} adsorbed in the valleys and humps, respectively. It has been demonstrated that the unoccupied states of C_{60} are more sensitive than the occupied states to charge transfer interactions with the substrate.[23,24] Due to the electron-accepting properties of C_{60} molecules, its unoccupied states have a tendency to hybridize with the surface states of the metal substrate. In accordance with these previous reports, the energy levels of the unoccupied states of C_{60} show significant variations depending on its adsorption sites. The downshift of 0.3 eV in the LUMO level toward the Fermi level signifies a greater degree of charge transfer to C_{60} molecules in the valley region, in agreement with the magnitude of orbital shift for one-electron transfer in the K_xC_{60} (x = 1, 2, 3, 4) system.[25] The corresponding dI/dV images show that the unoccupied states at 0.7 eV are mainly contributed by the C_{60} in the hump regions, while empty states at 0.4 eV primarily originate from the C_{60} in the valley regions. DFT calculations reveal that the amount of charge gained by C_{60} when it is located in the C_{hcp} valley is 0.210 e; it is 0.134 e in the C_{fcc} region, while on the graphene hump it is 0.143 e (Figure S6). Therefore, the preferential adsorption of C_{60} molecules on the C_{hcp} site can be traced to the partially ionic nature of the interactions.

The packing of the C_{60} molecules is examined as the thickness increases from a monolayer to multilayer in order to examine how the corrugation of the graphene Moiré superlattice affects 2D and 3D growth. On a smooth HOPG surface, C_{60} islands are observed to grow in a compact manner.[12] In contrast, dentritic islands with lobes, which are characteristic of diffusion-limited growth, are observed to grow on the graphene Moiré template for the first and second layer C_{60} films, and dentritic-to-compact growth occurs only in the third layer. Monolayer C_{60} islands are formed with their branches preferentially growing along the $\langle 01\bar{1}0\rangle$ directions and rotated by 120° with respect to each other (Figure 3d–f). The fastest growth direction aligns with the directions of the long diagonal in the unit cell of the Moiré pattern, forming a growth front rotated by 30° with respect to the <11$\bar{2}$0> directions in the Moiré superlattice (Figure 3f). These dendritic branches have their edge boundaries terminated at the Moiré hump regions, which results in a zigzag-type edge configuration (Figure S1). From the termination of the edges before the hump, we can infer that the graphene Moiré humps act as diffusion barriers. Nucleation of the second layer takes place when the first layer islands exceed a critical size (200 ± 20 nm). The second layer islands exhibit the same anisotropic growth behavior as the first layer islands (Figure 3d,e), which implies that the growth of the first two layers is influenced by the topography of the substrate. The influence of the substrate weakens significantly only when it comes to the growth of the third layer, where compact triangular islands that reflect the 3-fold

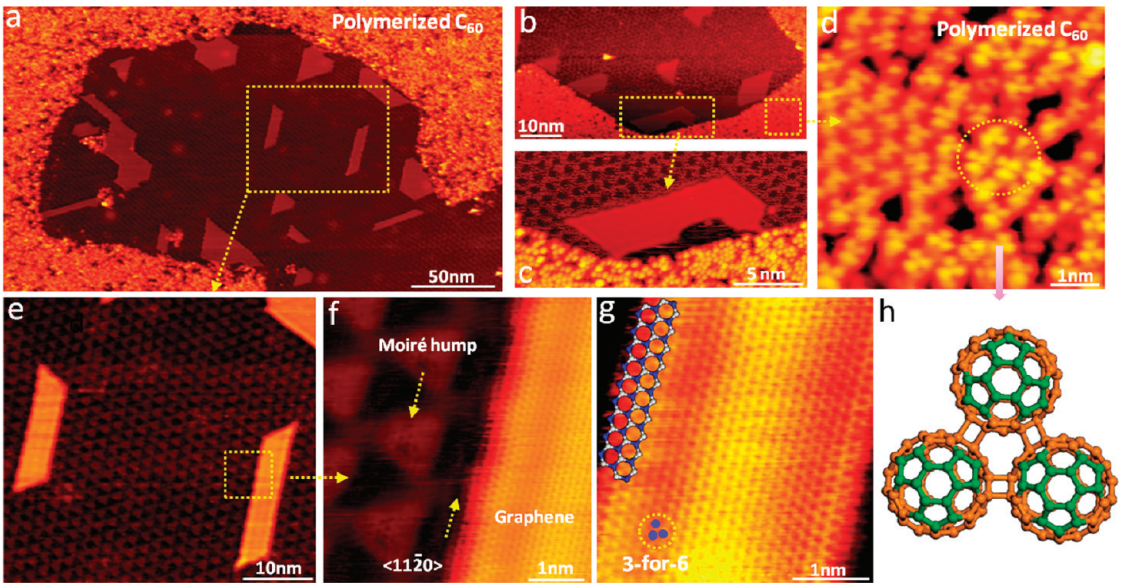

Figure 4. STM images of the homoepitaxy of graphene derived from flash annealing of multilayer dentritic C_{60} films on graphene Moiré pattern. (a–c) Series of STM images of polymerized C_{60} monolayer film and graphene nanostructures coexisting after flash annealing at 850 K. (d) Magnified view of the clover pattern for each C_{60} molecule in the polymerized film; the corresponding polymerization structure is shown in (h). (e) Homoepitaxial GNRs with well-defined edges coexist and surround the polymerized C_{60} film. (f) The edge of GNRs terminates in C_{hcp} valleys and aligns with $\langle 11\bar{2}0\rangle$ directions. (g) "3-for-6" triangular lattice observed in GNRs indicated in the yellow circle.

symmetry of the closed-packed C_{60}(111) surface (Figure 3e) are observed.

A closer inspection of the internal structures of the dentritic C_{60} islands (Figure 3) reveals interesting features about the layer-dependent crystallization process. A peculiar feature of the first layer C_{60} film is the presence of bright and dim spots arranged in a triangular symmetry that resembles the periodically corrugated graphene substrate (Figure 2a). The bright–dim pattern is inherited by the second layer, albeit with a gradual smearing in apparent corrugation. However, the specific bright–dim pattern is not observed in the third layer of C_{60} molecules, which indicates that the influence of the substrate on the growth of fullerite film is lost from the third layer onward (see Supporting Information for more details).

The morphology of the islands during 2D film growth is strongly influenced by the edge and corner diffusion of adsorbates as well as substrate–adsorbate interaction. The diffusion energy barrier from C_{hcp} to C_{fcc} valleys (along the $\langle 01\bar{1}0\rangle$ directions) is lower compared to that of C_{hcp} to a Moiré hump. The large lateral corrugation (ΔE_{ad} = 163 meV) in adsorption potential increases the energy barrier for edge migrations and favors the growth of fractal nanostructures. When the substrate temperature is increased to 450 K, the edge and corner diffusion become thermally activated and the fractal islands transform into compact islands (Figure S2), as judged by the increase in fractal dimension from 1.7 at RT to 2.0 at 450 K (based on the counting box method).[26] Finally, to prove the point that the substrate corrugation influences film growth, a simple modification of the corrugated graphene surface by the predeposition of a layer of planar coronene molecules now gives rise to the growth of compact C_{60} islands (Figure S2).

On the ruthenium surface, it is well known that C_{60} fragments can self-organize into a graphene monolayer at high temperature.[6] This motivates us to consider if the *epitaxial* growth of graphene could result from the assembly of C_{60}-derived fragments on top of the graphene Moiré pattern. To our delight, we observed that the homoepitaxial growth of graphene islands (Figure 4 and Figure S3) can be achieved by flash annealing multilayer dendritic C_{60} films on graphene at 850 K. As expected, the top C_{60} layers desorb completely during flash annealing. However, 20–30% of the graphene surface is still covered by monolayer C_{60} islands (Figure S3); this is retained from the bottom C_{60} layer, which has strong binding interactions with the graphene Moiré substrate. Magnified STM images (Figure 4d) reveal that C_{60} molecules now display a uniform 3-fold symmetry clover pattern (indicated in Figure 4h), which suggests that their rotations are blocked. The C_{60}–C_{60} intermolecular distance is reduced from 1 to 0.92 nm. These observations indicate that polymerization occurs among the surface-retained C_{60} molecules during flash annealing, which locks the C_{60} molecules into well-defined molecular orientations at RT. The polymerization of C_{60} molecules through [2 + 2] cycloaddition has been observed under high-temperature, high-pressure conditions or with electron beam radiation.[27,28]

The subsequent transformation of the polymerized C_{60} chains into an extended graphitic structure, such as carbon nanotubes, has also been documented.[28] From the images in Figure 4, it appears that the edges of the polymerized C_{60} film are unstable, and broken-off fragments act as solid precursors for the growth of graphene nanostructures. Figure 4a–c shows graphene trapezoids and nanoribbons growing at regions where the C_{60} polymerized film has decomposed. All the graphene nanostructures adopt a triangular lattice pattern with well-defined edge geometries (zigzag type) (Figure 4g). The triangular lattice is imaged as a "3-for-6" pattern (only three of the six carbon atoms in each hexagonal ring were imaged), which suggests that the graphene nanoribbon is commensurate with the underlayer graphene and follows the AB Bernal stacking instead of the incommensurate AA stacking, since the latter will cause a hexagonal honeycomb lattice to be imaged instead.[29] The graphene nanoribbons are observed (Figure 4e,f) to align with their zigzag edges parallel to the $\langle 11\bar{2}0\rangle$ directions, and the lack of in-plane rotation further confirms the commensurate AB stacking. In other words, this is a real epitaxy of graphene-on-graphene, in contrast to phase-segregated carbon atoms from the metal substrate, which will give rise to a disordered Moiré pattern (Figure S4). The reason for the growth of nanoribbons can be explained by the larger energy cost for the graphene edge to grow across the humps compared to growth along the valleys. Once the growth of the graphene edge initiates in specific $\langle 11\bar{2}0\rangle$ directions, which traverses across the valleys, the growth rate will be higher in this direction compared to the other equivalent $\langle 11\bar{2}0\rangle$ directions, as there is a high energy cost to climb over the humps, which leads to anisotropic growth. This suggests that the use of a corrugated or microscopically strained substrate where the surface symmetry is broken may promote anisotropic growth of crystals, due to topographical variation in diffusion barriers.

CONCLUSION

In summary, we show that the unique topography of the graphene Moiré superlattice allows the templated assembly of C_{60} molecules, which populate different microscopic regions in the hump and valley sites. Remarkably, due to the large trapping energy at the Moiré valleys, freezing of the molecular orientation and spatial alignment of individual C_{60} molecules can be attained at RT in this unique energy landscape. Such a highly oriented molecular array that is stable at RT may be potentially useful for applications in molecular spintronics, especially when endohedral fullerenes with magnetic spins can be aligned. The growth anisotropy of the C_{60} islands originates from the surface diffusion barriers on the landscape of humps and valleys, giving rise to the dendritic growth mode not seen on flat graphite surfaces. Our work also shows that the corrugation of the graphene lattice can be inherited by the growth of first and second layer molecular films. Due to the large surface trapping energies on the graphene Moiré template, C_{60} molecules undergo polymerization at elevated temperatures and act as a solid carbon precursor source for the homoepitaixal growth of graphene nanostructures.

METHODS

Experimental Procedures. The experiments were performed in an ultrahigh-vacuum (UHV) chamber with a base pressure of 2×10^{-10} mbar. A UHV STM unit (SPECS high temperature-STM 150 Aarhus) is employed for imaging and spectroscopy studies (Nanonis, SPECS Zurich SPM control system). The STM chamber is adjoined to a preparation chamber equipped with Knudsen cells (MBE-Komponenten, Germany) for the evaporation of C_{60}. During deposition, the substrate was held at room temperature. The deposition rate of C_{60} was calibrated by counting the coverage of the large-scale STM images with coverage below 1 monolayer (one layer of fully covered C_{60}). The clean Ru(0001) surface (Mateck) was prepared by repeated cycles of 1 keV-accelerated argon ion sputtering at room temperature with an argon pressure of 1×10^{-5} mbar. This was followed by annealing in an O_2 pressure of 2×10^{-7} mbar at 1000 K and subsequent flashing to 1600 K by e-beam heating. After sufficient treatment cycles, a clean Ru(0001) surface can be obtained. Subsequently, ethylene gas (National Oxygen Pte Ltd., purity 99.99%) at a partial pressure of 2.5×10^{-7} mbar was leaked into the chamber for 10 min on the Ru(0001) surface and the substrate was annealed at 800–1000 K in order to grow extended graphene covering the whole substrate by chemical vapor deposition.

Scanning Tunneling Spectroscopy (STS) Measurement and d*I*/d*V* Mapping. In addition to STM topographic images, the STS data were taken at 100 K to reduce the thermal noise. STS was performed using standard lock-in techniques to acquire d*I*/d*V* with a modulation voltage of 20–60 mV with a frequency of 2.4 kHz (Nanonis, SPECS Zurich SPM control system). The STS curve is an arithmetic average of values measured at 40–50 equally spaced points on C_{60} molecules.

Acknowledgment. This work is supported by NRF-CRP project "Graphene and Related Materials and Devices" (R-143-000-360-281).

Supporting Information Available: Supplementary data and figures. This material is available free of charge *via* the Internet at http://pubs.acs.org.

REFERENCES AND NOTES

1. Wang, Q. H.; Hersam, M. C. Room-Temperature Molecular-resolution Characterization of Self-Assembled Organic Monolayers on Epitaxial Graphene. *Nat. Chem.* **2009**, *1*, 206–211.
2. Dichtel, W. R.; Colson, J. W.; Woll, A. R.; Mukherjee, A.; Levendorf, M. P.; Spitler, E. L.; Shields, V. B.; Spencer, M. G.; Park, J. Oriented 2D Covalent Organic Framework Thin Films on Single-Layer Graphene. *Science* **2011**, *332* 228–231.
3. Champness, N. R.; Pollard, A. J.; Perkins, E. W.; Smith, N. A.; Saywell, A.; Goretzki, G.; Phillips, A. G.; Argent, S. P.; Sachdev,

H.; Muller, F.; *et al.* Supramolecular Assemblies Formed on an Epitaxial Graphene Superstructure. *Angew. Chem., Int. Ed.* **2010**, *49*, 1794–1799.
4. Hlawacek, G.; Khokhar, F. S.; van Gastel, R.; Poelsema, B.; Teichert, C. Smooth Growth of Organic Semiconductor Films on Graphene for High-Efficiency Electronics. *Nano Lett.* **2011**, *11*, 333–337.
5. Mao, J. H.; Zhang, H. G.; Jiang, Y. H.; Pan, Y.; Gao, M.; Xiao, W. D.; Gao, H. J. Tunability of Supramolecular Kagome Lattices of Magnetic Phthalocyanines Using Graphene-Based Moiré Patterns as Templates. *J. Am. Chem. Soc.* **2009**, *131*, 14136.
6. Lu, J.; Yeo, P. S. E.; Gan, C. K.; Wu, P.; Loh, K. P. Transforming C_{60} Molecules into Graphene Quantum Dots. *Nat. Nanotechnol.* **2011**, *6*, 247–252.
7. Barth, J. V. Molecular Architectonic on Metal Surfaces. *Annu. Rev. Phys. Chem.* **2007**, *58*, 375–407.
8. Barth, J. V.; Costantini, G.; Kern, K. Engineering Atomic and Molecular Nanostructures at Surfaces. *Nature* **2005**, *437*, 671–679.
9. Teichert, C.; Hlawacek, G.; Puschnig, P.; Frank, P.; Winkler, A.; Ambrosch-Draxl, C. Characterization of Step-Edge Barriers in Organic Thin-Film Growth. *Science* **2008**, *321*, 108–111.
10. Gravil, P. A.; Devel, M.; Lambin, P.; Bouju, X.; Girard, C.; Lucas, A. A. Adsorption of C-60 Molecules. *Phys. Rev. B* **1996**, *53*, 1622–1629.
11. Neek-Amal, M.; Abedpour, N.; Rasuli, S. N.; Naji, A.; Ejtehadi, M. R. Diffusive Motion of C_{60} on a Graphene Sheet. *Phys. Rev. E* **2010**, *82*, 051605.
12. Shin, H.; O'Donnell, S. E.; Reinke, P.; Ferralis, N.; Schmid, A. K.; Li, H. I.; Novaco, A. D.; Bruch, L. W.; Diehl, R. D. Floating Two-Dimensional Solid Monolayer of C_{60} on Graphite. *Phys. Rev. B* **2010**, *82*, 235427.
13. Wintterlin, J.; Bocquet, M. L. Graphene on Metal Surfaces. *Surf. Sci.* **2009**, *603*, 1841–1852.
14. Bocquet, M. L.; Wang, B.; Marchini, S.; Gunther, S.; Wintterlin, J. Chemical Origin of a Graphene Moiré Overlayer on Ru-(0001). *Phys. Chem. Chem. Phys.* **2008**, *10*), 3530–3534.
15. Donner, K.; Jakob, P. Structural Properties and Site Specific Interactions of Pt with the Graphene/Ru(0001) Moiré Overlayer. *J. Chem. Phys.* **2009**, *131*, 164701.
16. Sutter, E.; Albrecht, P.; Wang, B.; Bocquet, M. L.; Wu, L. J.; Zhu, Y. M.; Sutter, P. Arrays of Ru Nanoclusters with Narrow Size Distribution Templated by Monolayer Graphene on Ru. *Surf. Sci.* **2011**, *605*, 1676–1684.
17. Altenburg, S. J.; Kroger, J.; Wang, B.; Bocquet, M. L.; Lorente, N.; Berndt, R. Graphene on Ru(0001): Contact Formation and Chemical Reactivity on the Atomic Scale. *Phys. Rev. Lett.* **2010**, *105*, 236101.
18. Wasniowska, M.; Gyamfi, M.; Eelbo, T.; Wiesendanger, R. Inhomogeneous Electronic Properties of Monolayer Graphene on Ru(0001). *Phys. Rev. B* **2011**, *83*, 153418.
19. Yuan, L. F.; Wang, H. Q.; Zeng, C. G.; Li, Q. X.; Wang, B.; Hou, J. G.; Zhu, Q. S.; Chen, D. M.; Yang, J. L. Low-Temperature Orientationally Ordered Structures of Two-Dimensional C-60. *J. Am. Chem. Soc.* **2003**, *125*, 169–172.
20. Schull, G.; Berndt, R. Orientationally Ordered (7×7) Superstructure of C_{60} on Au(111). *Phys. Rev. Lett.* **2007**, *99*, 226105.
21. Muntwiler, M.; Auwarter, W.; Seitsonen, A. P.; Osterwalder, J.; Greber, T. Rocking-Motion-Induced Charging of C-60 on h-BN/Ni(111). *Phys. Rev. B* **2005**, *71*, 121402.
22. Nakamura, J.; Nakayama, T.; Watanabe, S.; Aono, M. Structural and Cohesive Properties of a C-60 Monolayer. *Phys. Rev. Lett.* **2001**, *87*, 048301.
23. Lu, X. H.; Grobis, M.; Khoo, K. H.; Louie, S. G.; Crommie, M. F. Spatially Mapping the Spectral Density of a Single C_{60} Molecule. *Phys. Rev. Lett.* **2003**, *90*, 0968021–0968024.
24. Grobis, M.; Lu, X.; Crommie, M. F. Local Electronic Properties of a Molecular Monolayer: C_{60} on Ag(001). *Phys. Rev. B* **2002**, *66*, 1614081–1614084.
25. Yamachika, R.; Grobis, M.; Wachowiak, A.; Crommie, M. F. Controlled Atomic Doping of a Single C_{60} Molecule. *Science* **2004**, *304*, 281–284.
26. Ogura, S.; Fukutani, K.; Matsumoto, M.; Okano, T.; Okada, M.; Kawamura, T. Dendritic to Non-dendritic Transitions in Au Islands Investigated by Scanning Tunneling Microscopy and Monte Carlo Simulations. *Phys. Rev. B* **2006**, *73*, 125442–125452.
27. Long, V. C.; Musfeldt, J. L.; Kamaras, K.; Adams, G. B.; Page, J. B.; Iwasa, Y.; Mayo, W. E. Far-Infrared Vibrational Properties of High-Pressure High-Temperature C_{60} Polymers and the C_{60} Dimer. *Phys. Rev. B* **2000**, *61*, 13191–13201.
28. Koshino, M.; Niimi, Y.; Nakamura, E.; Kataura, H.; Okazaki, T.; Suenaga, K.; Iijima, S. Analysis of the Reactivity and Selectivity of Fullerene Dimerization Reactions at the Atomic Level. *Nat. Chem.* **2010**, *2*, 117–124.
29. Hibino, H.; Mizuno, S.; Kageshima, H.; Nagase, M.; Yamaguchi, H. Stacking Domains of Epitaxial Few-layer Graphene on SiC(0001). *Phys. Rev. B* **2009**, *80*, 085408–085414.